

Localized hyperpolarizability approach to the origin of nonlinear optical properties in TeO₂-based materials

S. Suehara,^{1,*} P. Thomas,¹ A. P. Mirgorodsky,¹ T. Merle-Méjean,¹ J. C. Champarnaud-Mesjard,¹ T. Aizawa,² S. Hishita,² S. Todoroki,² T. Konishi,² and S. Inoue²

¹Laboratoire de Science des Procédés Céramiques et de Traitements de Surface (SPCTS)-UMR 6638 CNRS, 123 Avenue, Albert Thomas, 87060 Limoges, France

²Advanced Materials Laboratory, National Institute for Materials Science, 1-1 Namiki, Tsukuba, Ibaraki 305-0044, Japan

(Received 16 June 2003; revised manuscript received 25 February 2004; published 16 November 2004)

We present an *ab initio* molecular orbital theoretical approach to the origin of nonlinear optical (NLO) properties in the TeO₂-based materials from the viewpoint of “electron pairs” assigned to the individual chemical bond. Localized static dipole moments, linear polarizabilities, and hyperpolarizabilities of the individual chemical bonds in the TeO₄ and TeO₃ structural units are calculated in terms of the localized molecular orbitals. While no significant difference is found between these structural units in both the static bond dipole moment and the linear polarizability, the hyperpolarizabilities exhibit large differences. The TeO₄ structural unit shows much higher second hyperpolarizability than the TeO₃ structural unit. It is shown that the lone pair of the electrons on Te atom has the very large nonlinear response property, which should cause the high third-order NLO efficiency of the TeO₂-based materials. Geometric dependency of the second hyperpolarizability is also discussed on the basis of the calculations on the several deformed structural units.

DOI: 10.1103/PhysRevB.70.205121

PACS number(s): 31.15.Ar, 42.25.Ja, 42.65.An

I. INTRODUCTION

Optical response of a dielectric material can be described by the polarization (P), which is induced to oscillate by the electric field component (E) of the light injected under the condition that the wavelength of the light is very much longer than the dimensions of the unit cells of the material and the interaction between the magnetic field component of the light and the material is ignored. Since the oscillation of P , i.e., the charge vibration, is responsible for the propagation of light and determines the observed optical frequencies, knowing how P responds with respect to E and which factor characterizes it are very important for understanding the dielectric material. At present, the nonlinear behavior of $P(E)$ is of considerable interest in the optical material research field because it leads to various nonlinear optical (NLO) effects such as Kerr and Pockels effects, second- and third-harmonic generations, etc. These NLO properties should be applicable to optical signal-processing, optical computing, and the other optical functional devices.

$P(E)$ can be defined by

$$P(E) = \sum_i \mu_i(E), \quad (1)$$

where $\mu_i(E)$ is the dipole moment of the component part i , which consists of an ionic core (positive charge) and a negative charge center by electrons surrounding the ionic core in a dielectric material. In general, the dipole $\mu_i(E)$ does not respond linearly. Its behavior relates to the electronic and structural properties of the material such as band gap, atomic radius, bond length, symmetry, etc.¹⁻⁵ While revealing and describing nonlinear phenomena using these parameters are generally very complicated, Levine has proposed a simple, electrodynamic picture called “bond additivity model” or “bond parameter model.”^{6,7} This model emphasizes that the

anharmonic motion of the “localized-bond charge,” which was determined empirically, causes NLO properties and is validated for calculating the linear and nonlinear susceptibilities of the various crystal structures.⁸ Here, we present an *ab initio* molecular orbital (MO) theoretical approach to the origin of NLO properties in TeO₂-based materials from the viewpoint of “electron pairs” which can be closely related to the localized-bond charge. This work will offer a kind of the bond additivity model with use of first-principles calculation.

The TeO₂-based materials exhibit high third order NLO susceptibilities and are regarded as the promising NLO materials.⁹⁻¹¹ Recently, a number of experimental and theoretical studies have been performed on the structure of TeO₂-based materials. These studies have revealed that the TeO₂-based materials almost consist of two structural units: a TeO₄ trigonal bipyramid polyhedron and a TeO₃ trigonal pyramid one,¹²⁻¹⁷ and that the TeO₄ structural unit may be responsible for the high third order NLO properties rather than the TeO₃ one in both crystals and glasses of the TeO₂-based compounds.^{18,19}

In this paper, we focus mainly on the origin of the difference between these typical structural units with respect to the linear polarizability (α) and the second hyperpolarizability (γ) of both their entirety and the individual chemical bonds.

II. CALCULATION

In order to calculate the (hyper)polarizabilities of TeO₄ and TeO₃ structural units, we optimized the structure of hydrogen-terminated clusters, TeO₄H₄ and TeO₃H₃⁺ by using density functional theory (DFT) calculations. Becke’s three parameter hybrid method²⁰ using the Lee-Yang-Parr²¹ and Vosko-Wilk-Nusair²² formula V correlation functionals (B3LYP) was employed in the DFT calculations.²³ It is well known that the calculation of (hyper)polarizabilities requires

TABLE I. Effects of basis set augmentation on the isotropic linear polarizability $\langle\alpha\rangle$, second hyperpolarizability $\langle\gamma\rangle$, total energy, and Te-O bond length of the optimized TeO_4H_4 geometry. Added diffuse sp and polarization d functions to the SBKJC standard basis set are denoted in brackets. $\zeta_{\text{diff}}^{\text{Te}}$ and $\zeta_{\text{pol}}^{\text{O}}$ show the exponents of the diffuse sp and polarization d functions, respectively, for Te and O.

Basis set	$\langle\alpha\rangle^a$ (a.u.)	$\langle\gamma\rangle^a$ (a.u.)	Energy ^b (a.u.)	Te-O bond length ^c (nm)	$\zeta_{\text{diff}}^{\text{Te}}/\zeta_{\text{diff}}^{\text{O}}$ ^d ($\times 10^{-2}$)	$\zeta_{\text{pol}}^{\text{Te}}/\zeta_{\text{pol}}^{\text{O}}$ ^e ($\times 10^{-1}$)
SBKJC	50.3	3500	-74.120	0.204/0.204		
SBKJC(d)	49.8	3231	-74.227	0.203/0.196		2.37/8.00
SBKJC(sp)	59.3	11328	-74.138	0.204/0.204	3.06/8.45	
SBKJC(sp,d)	57.4	11257	-74.240	0.203/0.197	3.06/8.45	2.37/8.00
SBKJC($sp,2d$)	59.4	11333	-74.265	0.202/0.196	3.06/8.45	3.32,0.95/11.20,3.20 ^f
SBKJC($sp,3d$)	60.2	11858	-74.280	0.203/0.196	3.06/8.45	7.11,2.37,0.79/24.00,8.00,2.67 ^f

^aFor extracting energy-based $\langle\alpha\rangle$ and $\langle\gamma\rangle$, the B3LYP calculations under the applied electric fields of $(e,0,0)$, $(0,e,0)$, $(0,0,e)$, $(e,e,0)$, $(e,0,e)$, $(0,e,e)$, $(e,-e,0)$, $(0,e,-e)$, and $(-e,0,e)$ were performed with $e = 0.000, \pm 0.010, \pm 0.020$ a.u. We confirmed that the calculations with ten times lower electric fields ($e = 0.000, \pm 0.001$ and ± 0.002 a.u.) give less important differences (less than $\sim 0.01\%$ and $\sim 6\%$ for $\langle\alpha\rangle$ and $\langle\gamma\rangle$, respectively, at each basis set).

^bThe total energy for the optimized geometry without external electric field.

^cThe geometry was optimized using analytic energy gradients at each basis set without external electric field. A typical TeO_4 structural unit has two kinds of Te-O bond. For example, Te-O bond lengths of the α - TeO_2 crystal are of 0.188 and 0.212 nm. Therefore, two types of the Te-O bond are indicated here.

^dFrom Refs. 33 and 46.

^eFrom Refs. 33 and 47.

^fDerived from the single ζ_{pol} (Te:0.237, O:0.800) value using the splitting factors (1.4, 0.4 for $2d$, and 3.00, 1.00, 0.333 for $3d$ polarization functions).³³

large basis sets and extraordinary accuracy in the wave function while replacing the core electrons with an effective core potential (ECP) does not reduce the accuracy of (hyper)polarizabilities.^{24–26} We used the ECP and valence basis set by Stevens, Basch, Krauss, Jasien, and Cundari (SBKJC)^{27–29} with extra basis augmentation. In order to obtain an adequate basis set augmentation, we performed the preliminary convergence study on the TeO_4H_4 cluster. In the self-consistent field (SCF) cycles, HONDO/Rys³⁰ integrals were used and the integrals less than 10^{-20} were ignored. We took the SCF density convergence criterion as 10^{-10} . The above treatment gives high integral and wave function accuracy.²⁴ Table I shows the effects of the basis set on the calculational results. The isotropic polarizabilities are deduced from the total energy calculations. SBKJC basis set without any augmentation does not reproduce two kinds of the Te-O bond: the long and short Te-O bonds found in α - TeO_2 crystal.³¹ SBKJC(d) basis set reproduces two kinds of the Te-O bond, but it still fails to give the sufficient polarizability convergences. On the other hand, the SBKJC(sp) basis set gives adequate saturation of polarizabilities although it cannot reproduce the Te-O bond length splitting. It should be noted that a better variational energy seems to give the more reasonable structure but does not necessarily imply an improved description for (hyper)polarizability. The basis sets augmented by both the diffuse sp and polarization d functions give reasonable values for not only polarizabilities but also for Te-O bond length splitting. The differences of polarizabilities and Te-O bond length are less than $\sim 5\%$ and $\sim 0.5\%$, respectively. In the following calculation, we employed the SBKJC($sp,3d$) basis set.

Of particular concern in the present work are the dipole moments of the chemical bonds defined by electron pairs. Individual chemical bond was determined based on the energy localized molecular orbital (LMO) by Edmiston and Ruedenberg and a Mulliken type analysis of it.^{32,33} In general, delocalized MOs, namely canonical MOs, have complicated shapes spreading into a whole molecule. The energy LMOs are derived from them by the orthogonal transformation to have a maximum orbital self-energy. Total energy is invariant in the transformation since a Slater determinant wave function is unchanged by unitary transformation of MOs. The localization procedure results in minimizing the Coulomb interaction between one LMO to the others. An energy LMO corresponds to a bonding pair (bp) or lone pair (lp) of electrons because the procedures of “maximizing the orbital self-energies” and “minimizing the Coulomb interactions” are associated with “making electron pairs” and “minimizing the repulsion energy between electron pairs,” respectively. The energy-LMO method offers the similar electron pairs configuration as given by the valence shell electron pair repulsion (VSEPR) theory.³⁴

A bond dipole moment μ_i of the chemical bond i was calculated from the combination of two electrons in the LMO i and two point charges traced to the divided nucleus charges (so-called “localized nuclear charges”). The two point charges are distributed as follows: if the electron pair in the LMO is a lp, they are assigned to the nucleus to which the lp belongs. If it is a bp, one point charge is assigned to each of the two nuclei belonging to the bond.³⁵ Then, μ_i can be written by

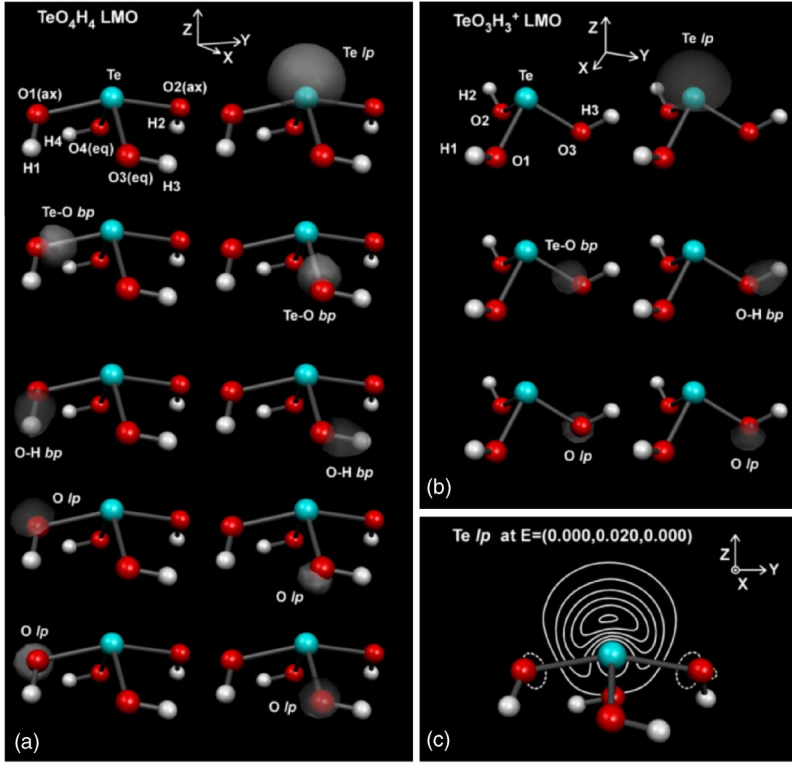


FIG. 1. (Color online) Optimized geometries and LMOs at $E=(0,0,0)$ for (a) TeO_4H_4 and (b) TeO_3H_3^+ . (c) LMO of Te lp of TeO_4H_4 under the applied field of $E_y=0.02$ a.u. The optimized geometry of TeO_4H_4 is as follows: $\text{Te-O1}=\text{Te-O2}=0.203$ nm, $\text{Te-O3}=\text{Te-O4}=0.196$ nm, $\text{O1-H1}=\text{O2-H2}=0.098$ nm, $\text{O3-H3}=\text{O4-H4}=0.098$ nm, $\angle\text{O1-Te-O2}=160.0$ deg, $\angle\text{O3-Te-O4}=107.6$ deg, $\angle\text{Te-O1-H1}=\angle\text{Te-O2-H2}=111.0$ deg, and $\angle\text{Te-O3-H3}=\angle\text{Te-O4-H4}=106.4$ deg. Cartesian x , y , and z axes are taken as shown in this figure where y and z axes are parallel to the O1-O2 line and C_2 symmetric rotational axis, respectively. The y direction and the xz plane are often called “the axial direction” and “the equatorial plane” in this geometry. The optimized geometry of TeO_3H_3^+ is as follows: $\text{Te-O1}=\text{Te-O2}=\text{Te-O3}=0.190$ nm, $\text{O1-H1}=\text{O2-H2}=\text{O3-H3}=0.098$ nm, $\angle\text{O1-Te-O2}=\angle\text{O2-Te-O3}=\angle\text{O3-Te-O1}=92.0$ deg, and $\angle\text{Te-O1-H1}=\angle\text{Te-O2-H2}=\angle\text{Te-O3-H3}=115.3$ deg. The LMOs identical to the displayed ones were omitted. All three-dimensional rendering graphics visualization of these orbitals were made by the MOLEKEL software.⁴⁸

$$\mu_i = e(R_i + R'_i) - 2er_i,$$

where e is the elementary electric charge, both R_i and R'_i are the position vectors of two point charges assigned to the LMO i , and r_i is the center position of the electron pair defined with LMO wave function ϕ_i by

$$r_i = \int |\phi_i|^2 r dr.$$

Each of the x , y , and z components of the dipole moments $\mu_{i,j}$ ($j=x,y,z$) of chemical bond i was calculated under the applied electric field $\mathbf{E}(E_x, E_y, E_z)=(e, 0, 0)$, $(0, e, 0)$, $(0, 0, e)$, $(e, e, 0)$, $(e, 0, e)$, $(0, e, e)$, $(e, -e, 0)$, $(0, e, -e)$, and $(-e, 0, e)$ with $e=0.000, \pm 0.005, \pm 0.010, \pm 0.015$, and ± 0.020 in atomic units (a.u.). The z axis was taken as the principal rotation axis of both TeO_4H_4 and TeO_3H_3^+ cluster models. The applied electric field strengths were determined by supposing the maximum practical electric field for usual NLO experiments in the order of 10^{10} V/m (~ 0.020 a.u.).^{36,37} It was confirmed that (hyper)polarizabilities do not depend on the electric field strength (see the footnote in Table I).

The localized linear polarizability $\alpha_{i,jk}$, first hyperpolarizability $\beta_{i,jkl}$, and second hyperpolarizability $\gamma_{i,jklm}$ ($j,k,l,m=x,y,z$), which are the tensile (hyper)polarizability components of the chemical bond i , were derived numerically from least-squares fitting of the fourth-order dipole moment function described by a Taylor series in powers of E :

$$\begin{aligned} \mu_{i,j} = & \mu_{i,j}^{\text{static}} + \sum_k \alpha_{i,jk} E_k + \frac{1}{2!} \sum_{kl} \beta_{i,jkl} E_k E_l \\ & + \frac{1}{3!} \sum_{klm} \gamma_{i,jklm} E_k E_l E_m + \frac{1}{4!} \sum_{klmn} \delta_{i,jklmn} E_k E_l E_m E_n \end{aligned}$$

to the bond dipole moment values $\mu_{i,j}$ under $\mathbf{E}(E_x, E_y, E_z)$ with the fitting parameters $\mu_{i,j}^{\text{static}}$, $\alpha_{i,jk}$, $\beta_{i,jkl}$, $\gamma_{i,jklm}$, and $\delta_{i,jklmn}$. As our target materials are centrosymmetric crystals and glasses of the TeO_2 -based compounds, the isotropic average well corresponds to the real situations. The isotropic average values are²

$$\langle \alpha_i \rangle = \frac{1}{3} (\alpha_{i,xx} + \alpha_{i,yy} + \alpha_{i,zz})$$

$$\begin{aligned} \langle \gamma_i \rangle = & \frac{1}{5} (\gamma_{i,xxxx} + \gamma_{i,yyyy} + \gamma_{i,zzzz} + \gamma_{i,xxyy} + \gamma_{i,yyzz} + \gamma_{i,zzxx} \\ & + \gamma_{i,yyxx} + \gamma_{i,zzyy} + \gamma_{i,xxzz}). \end{aligned}$$

All B3LYP/SBKJC($sp, 3d$) calculations including Edmiston-Ruedenberg energy localization of canonical MOs were performed with the quantum chemistry code GAMESS³³ at the National Institute for Materials Science (Namiki, AlphaServer GS140/COMPAQ) and the Laboratory of Science des Procédés Céramiques et de Traitements de Surface (Limoges, GT9000/SAMSUNG). The numerical fitting process to calculate (hyper)polarizability over LMO was executed by a separate code written in Python³⁸ script language.

III. RESULTS

The optimized C_2 symmetric geometry of TeO_4H_4 and the LMOs are shown in Fig. 1(a). Two kinds of Te-O bonds, i.e.,

TABLE II. Localized static bond dipole moments $|\mu^{\text{static}}|$ (a.u.) for the TeO_4H_4 and TeO_3H_3^+ cluster models.

Electron pair	$\text{TeO}_4\text{H}_4^{\text{a}}$	TeO_3H_3^+
Te lp	2.3	2.2
Te-O bp ^b	1.7 [1.9/1.6]	1.4
O lp	1.1 [1.1/1.1]	1.0
O-H bp	0.1 [0.1/0.1]	0.5

^aAs for $|\mu^{\text{static}}|$ in TeO_4H_4 , the average values of those that are traced to O(ax) and O(eq) are shown with the individual values in the square brackets formatted as [O(ax)-related/O(eq)-related].

^bTe-O bond lengths for TeO_4H_4 and TeO_3H_3^+ are of 0.200 [0.203/0.196] and 0.190 nm, respectively.

the long Te-O(ax) (0.203 nm) and the short Te-O(eq) (0.196 nm) were reproduced making the trigonal bipyramid configuration. The optimized C_3 symmetric geometry of TeO_3H_3^+ and its LMOs are shown in Fig. 1(b). It consists of one central Te atom and three equivalent O atoms (O1, O2, and O3) at 0.190 nm. The primary common feature of the TeO_3 structural units among many TeO_2 -based materials is the trigonal pyramid with the shorter Te-O bond length than ones in the Te-O_4 structural unit. Most experiments reported the Te-O bond length in the TeO_3 structural units to be 0.183–0.190 nm.^{39–43} The optimized geometry gives a reasonable model of the TeO_3 structural units. The LMOs of both clusters were fairly well localized and correspond to the respective electron pairs.

The individual electron pairs in the TeO_4H_4 and TeO_3H_3^+ cluster models can be classified into four kinds: Te lp, Te-O bp, O lp, and O-H bp. Localized static dipole moments, linear polarizabilities, and second hyperpolarizabilities of each kind are listed in Tables II, III, and IV, respectively. As for Te-O bp, O lp, and O-H bp in TeO_4H_4 , the average values of those that are traced to two types of oxygen, i.e., O(ax) and O(eq), are shown with the individual values in the square brackets in Tables II and III. In Table IV, the off-axial components of γ are omitted because these values are generally less than the axial components. The cluster total (hyper)polarizabilities and the reduced ones to TeO_2 are also shown in Tables III and IV. The reduced TeO_2 value corresponds to one for a “ TeO_2 ” fragment in bulk, i.e., the sum of the localized (hyper)polarizability for Te lp \times 1, Te-O bp \times 4, and

TABLE III. Isotropic linear polarizabilities $\langle\alpha\rangle$ (a.u.) for the TeO_4H_4 and TeO_3H_3^+ cluster models.

Electron pair	$\text{TeO}_4\text{H}_4^{\text{a}}$	TeO_3H_3^+
Te lp	11.7	10.6
Te-O bp	4.1 [4.4/3.9]	3.6
O lp	3.1 [3.2/3.1]	3.1
O-H bp	1.8 [1.9/1.6]	1.7
Cluster	60.2	45.1
Red. TeO_2	40.7	37.3

^aAs for $\langle\alpha\rangle$ in TeO_4H_4 , the average values of those that are traced to O(ax) and O(eq) are shown with the individual values in the square brackets formatted as [O(ax)-related/O(eq)-related].

O lp \times 4. From the stoichiometric point of view, the reduced TeO_2 values should be meaningful rather than the values for a cluster or a structural unit, since most of TeO_2 -based materials are described by a formula of $n\text{M}_x\text{O}_y\cdot m\text{TeO}_2$ (n, m, x, y ; numbers, M; a modifier element).

IV. DISCUSSION

As seen in Figs. 1(a) and 1(b), spatial distribution of the LMO resembles each other between TeO_4H_4 and TeO_3H_3^+ . This is also true in the static bond dipole moment $|\mu|$ shown in Table II. Especially, $|\mu(\text{Te lp})|$ of TeO_4H_4 and TeO_3H_3^+ have large values of 2.3 and 2.2 a.u., respectively, which are derived from the Te lp located at a distance of ~ 0.06 nm from the Te core along z axis. The feature of Te lp is consistent with the VSEPR theory: shorter distance between Te core and lp than the Te-O bond lengths (~ 0.190 nm) and larger area lp spread than bp around Te atom, although the structurally estimated Te core-lp distance of 0.138 nm by Thomas³¹ is somehow larger than the present value. In the LMO view, the Te lps have almost all the same atomic orbital components in both TeO_4H_4 and TeO_3H_3^+ . These Te lps are mainly made up of the s orbital admixed with the p and d orbitals of Te atom. The $s:p:d$ mixture ratios of Te lps derived from the LMO coefficients are of 1.2:0.5:0.3 and 1.1:0.5:0.3 for TeO_4H_4 and TeO_3H_3^+ , respectively. Te-O bond dipole moment $|\mu(\text{Te-O bp})|$ varies with the bond

TABLE IV. Axial components of γ and $\langle\gamma\rangle$ (a.u.) for the TeO_4H_4 and TeO_3H_3^+ cluster models.

Electron pair	TeO_4H_4				TeO_3H_3^+			
	γ_{xxxx}	γ_{yyyy}	γ_{zzzz}	$\langle\gamma\rangle$	γ_{xxxx}	γ_{yyyy}	γ_{zzzz}	$\langle\gamma\rangle$
Te lp	1702	4375	4603	3746	700	701	1577	1142
Te-O bp	549	1744	978	1113	210	205	675	406
O lp	795	554	541	681	328	331	233	310
O-H bp	−41	73	−12	−3	63	58	−57	14
Cluster	10101	16075	12796	13632	3488	3480	4830	4264
Red. TeO_2	7082	13565	10679	10920	2854	2847	5209	4007

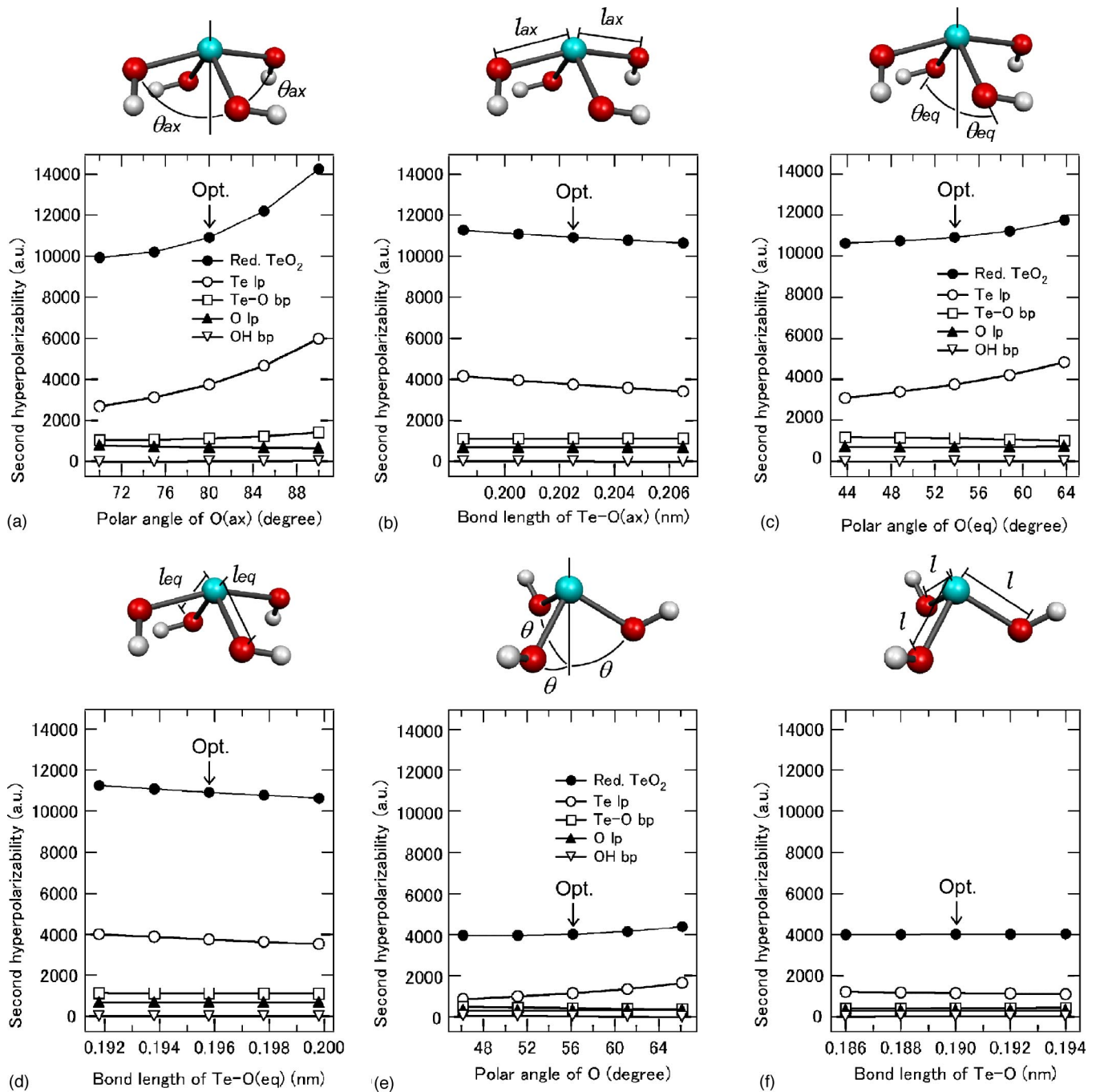


FIG. 2. (Color online) Reduced TeO_2 and localized second hyperpolarizabilities for the TeO_4H_4 clusters deformed in (a) $\text{Te-O}_{(\text{ax})}$ polar angle, (b) $\text{Te-O}_{(\text{eq})}$ polar angle, (c) $\text{Te-O}_{(\text{ax})}$ bond length, and (d) $\text{Te-O}_{(\text{eq})}$ bond length, and for the TeO_3H_3^+ clusters deformed in (e) Te-O polar angle and (f) Te-O bond length. The geometric parameters for the optimized structure are indicated by the arrows.

length as shown in Table II, which should indicate some ionic feature in this bond. The small values of $|\mu(\text{O-H bp})|$ in TeO_4H_4 and TeO_3H_3^+ are associated with the electron pairs staying in the middle position between O and H cores, suggesting typical covalent bonding.

In Table III, the highest linear polarizability is assigned to Te lp, and Te-O bp and O lp follow it in both cluster models. O-H bp has similar value and is smaller than the others. The TeO_4H_4 cluster has higher linear polarizability than the TeO_3H_3^+ . This is mainly caused by the difference in the num-

ber of the total electrons of the clusters. The linear polarizability of TeO_4H_4 approximately consists of TeO_3H_3^+ plus one (Te)-O-H bond. The reduced TeO_2 linear polarizability indicates small difference between TeO_4H_4 and TeO_3H_3^+ .

In Table IV, TeO_4H_4 exhibits higher $\langle\gamma\rangle$ than TeO_3H_3^+ even in the reduced value. The larger $\langle\gamma(\text{red. TeO}_2)\rangle$ of TeO_4H_4 than of TeO_3H_3^+ is consistent with the experimental fact that the more TeO_3 structural units in a tellurite glass, the less its nonlinearity.¹⁸ The large second hyperpolarizability of TeO_4H_4 is mainly originated from γ_{yyyy} which indi-

cates that third-harmonic generation ($\omega \rightarrow 3\omega$) will occur most effectively when the light is injected with alternating electric field along axial direction (y axis) in the TeO_4 geometry.

The localized second hyperpolarizabilities $\langle \gamma(\text{Te lp}) \rangle$, $\langle \gamma(\text{Te-O bp}) \rangle$ and $\langle \gamma(\text{O lp}) \rangle$ of TeO_4H_4 are over two times higher than those of TeO_3H_3^+ . This is quite different from the tendency of the localized dipole moment and linear polarizability discussed above. As for O-H bp, there are small differences between the cluster models. In both clusters, $\langle \gamma(\text{Te lp}) \rangle$ shows the larger value than $\langle \gamma(\text{Te-O bp}) \rangle$ and $\langle \gamma(\text{O lp}) \rangle$. The displacement of the Te lp of TeO_4H_4 under the electric field less than 0.020 a.u. is not so large: 0.013, 0.013, and 0.012 nm for $\mathbf{E}(e, 0, 0)$, $\mathbf{E}(0, e, 0)$, and $\mathbf{E}(0, 0, e)$ with $e=0.02$ a.u., respectively. We show the LMO contour map of Te lp at $\mathbf{E}(0, 0.02, 0)$ in Fig. 1(c) for example. These small displacements under rather large macroscopic field of 0.02 a.u. should originate from larger microscopic Coulomb field (~ 1 a.u.) governing the binding between electrons and cores. This may indicate the availability of perturbation method in time-dependent (TD) HF and TD-DFT.^{44,45}

The present results have shown that the Te lp has no significant differences between the TeO_4 and TeO_3 structural units in terms of their static dipole moments, linear polarizabilities, and orbital components, although the localized hyperpolarizabilities exhibit large differences. This may refer a transferability limit of the properties derived from the individual chemical bonds to the other system with respect to the optical parameters. Our results suggest that similar linear polarizability is expected in the materials having similar chemical bonds. This manner, however, should have poor transferability within the hyperpolarizabilities. The most likely explanation for this is that the primary parabolic potential shape stimulating the dipole responding linearly can be characterized inside the individual chemical bond, whereas the distortion of the potential from the parabolic shape should be caused by neighboring chemical bond. As this distortion is reflected in the localized hyperpolarizabilities, it is essential to take the local geometry into consideration for estimating the hyperpolarizabilities.

Since the local structures are close to but different from the present optimized geometries in the real TeO_2 -based materials, it is worth looking over the geometric dependency of the localized second hyperpolarizabilities. Finally, we show the localized and reduced TeO_2 second hyperpolarizabilities for several deformed TeO_4 and TeO_3 structural units from the energetically optimized ones. Since so many deformed structures are suggested that calculating all of them is beyond our limited computational resources, we restrict the deformation as follows: (1) Symmetries of the TeO_4H_4 and

TeO_3H_3^+ cluster models are kept. (2) The deformation parameters are the Te-O bond length and the polar angle of Te-O bonds with respect to z axis. (3) Only one parameter varies from the optimized structure (the other parameters are fixed to the values in the optimized geometry). (4) O-H bonds are unchanged (i.e., each of H atoms is stuck in and follows the respective O atom in the deformation procedures). The deformation parameters of the polar angle and the bond length are varied with 5 deg and 0.002 nm steps, respectively.

The reduced and localized TeO_2 second hyperpolarizabilities of the deformed structures are shown in Fig. 2. In both TeO_4H_4 and TeO_3H_3^+ deformed structures, the $\langle \gamma(\text{red. TeO}_2) \rangle$ changes following $\langle \gamma(\text{Te lp}) \rangle$ while $\langle \gamma(\text{Te-O bp}) \rangle$, $\langle \gamma(\text{O lp}) \rangle$, and $\langle \gamma(\text{O-H bp}) \rangle$ remain at much smaller values, suggesting that Te lp is a key of the NLO properties of the tellurite materials. Increasing the polar angle of O and shortening the Te-O bond makes the NLO response of Te lp larger. It seems to be a reasonable view from this that $\langle \gamma(\text{Te lp}) \rangle$ is very sensitive to the distance between Te lp and the other electron pairs and cores: Te-O bps, O lps, and oxygen cores. These results provide useful insight into the structure-NLO property relationships in TeO_2 -based materials.

V. SUMMARY

Localized static dipole moments, linear polarizabilities, and hyperpolarizabilities assigned to the individual chemical bonds in the TeO_4 and TeO_3 structural units of the TeO_2 -based materials were presented by the *ab initio* MO calculations with use of the LMO analysis. While no significant difference was found in terms of the static bond dipole moment and the localized linear polarizability between these structural units, the localized second hyperpolarizabilities showed large difference. The TeO_4 structural unit exhibits much higher second hyperpolarizability than the TeO_3 structural unit. The origin of the high NLO properties of the TeO_2 -based materials should be attributed to the Te lp in TeO_4 structural unit that has very large third order nonlinear response property. From the second hyperpolarizability calculations on several deformed structures, it was suggested that Te lp is very sensitive to the distance between Te lp and the other electron pairs and cores.

ACKNOWLEDGMENTS

One of the authors (S.S.) wishes to thank Professor Toshiaki Osaka (Waseda University), Yuki Miwa (NIMS), and Dr. M. B. Smirnov (Institute for Silicate Chemistry of RASc.) for their support and encouragement through this work.

*On leave from FGG-AML, National Institute for Materials Science, Tsukuba, Ibaraki 305-0044, Japan. Email address: suehara.shigeru@nims.go.jp

¹M. E. Lines, Phys. Rev. B **41**, 3383 (1990).

²T. R. Cundari, H. A. Kurtz, and T. Zhou, Chem. Phys. **240**, 205 (1999).

³P. P. Korambath and S. P. Karna, J. Phys. Chem. A **104**, 4801 (2000).

- ⁴D. Xue and S. Zhang, *J. Phys. Chem. Solids* **59**, 1337 (1998).
- ⁵N. Bloembergen and Y. R. Shen, *Phys. Rev.* **133**, A37 (1964).
- ⁶B. F. Levine, *Phys. Rev. Lett.* **22**, 787 (1969).
- ⁷Y. R. Shen, *The Principles of Nonlinear Optics* (Wiley Interscience, New York, 1984).
- ⁸B. F. Levine, *Phys. Rev. B* **7**, 2600 (1973).
- ⁹E. M. Vogel, M. J. Weber, and D. M. Krol, *Phys. Chem. Glasses* **32**, 231 (1991).
- ¹⁰H. Nasu, Y. Ibara, and K. Kubodera, *J. Non-Cryst. Solids* **110**, 229 (1989).
- ¹¹S.-H. Kim, T. Yoko, and S. Sakka, *J. Am. Ceram. Soc.* **76**, 2486 (1993).
- ¹²T. Uchino and T. Yoko, *J. Non-Cryst. Solids* **204**, 243 (1996).
- ¹³S. Suehara, K. Yamamoto, S. Hishita, and A. Nukui, *Phys. Rev. B* **50**, 7981 (1994).
- ¹⁴S. Suehara, K. Yamamoto, S. Hishita, T. Aizawa, S. Inoue, and A. Nukui, *Phys. Rev. B* **51**, 14919 (1995).
- ¹⁵Y. Himei, Y. Miura, T. Nanba, and A. Osaka, *J. Non-Cryst. Solids* **211**, 64 (1997).
- ¹⁶S. Suehara, S. Hishita, S. Inoue, and A. Nukui, *Phys. Rev. B* **58**, 14124 (1998).
- ¹⁷H. Niida, T. Uchino, J. Jin, S.-H. Kim, T. Fukunaga, and T. Yoko, *J. Chem. Phys.* **114**, 459 (2001).
- ¹⁸B. Jeansannetas, S. Blanchandin, P. Thomas, P. Marchet, J. C. Champarnaud-Mesjard, T. Merle-Méjean, B. Frit, V. Nazabal, E. Fargin, G. L. Flem *et al.*, *J. Solid State Chem.* **146**, 329 (1999).
- ¹⁹A. Berthereau, E. Fargin, A. Villezusanne, R. Olazcuaga, G. L. Flem, and L. Ducasse, *J. Solid State Chem.* **126**, 143 (1996).
- ²⁰A. D. Becke, *J. Chem. Phys.* **98**, 5648 (1993).
- ²¹C. Lee, W. Yang, and R. G. Parr, *Phys. Rev. B* **37**, 785 (1988).
- ²²S. H. Vosko, L. Wilk, and M. Nusair, *Can. J. Phys.* **58**, 1200 (1980).
- ²³R. H. Hertwig and W. Koch, *Chem. Phys. Lett.* **268**, 345 (1997).
- ²⁴T. R. Cundari, H. A. Kurtz, and T. Zhou, *J. Phys. Chem. A* **102**, 2962 (1998).
- ²⁵S. P. Karna, and M. Dupuis, *J. Chem. Phys.* **92**, 7418 (1990).
- ²⁶S. P. Karna and M. Dupuis, *Chem. Phys. Lett.* **171**, 201 (1990).
- ²⁷W. J. Stevens, H. Basch, and M. Krauss, *J. Chem. Phys.* **81**, 6026 (1984).
- ²⁸W. J. Stevens, M. Krauss, H. Basch, and P. G. Jasien, *Can. J. Phys.* **70**, 612 (1992).
- ²⁹T. R. Cundari and W. J. Stevens, *J. Chem. Phys.* **98**, 5555 (1993).
- ³⁰M. Dupuis, J. D. Watts, H. O. Villar, and G. J. B. Hurst, *Comput. Phys. Commun.* **52**, 415 (1989).
- ³¹P. A. Thomas, *J. Phys. C* **21**, 4611 (1988).
- ³²C. Edmiston and K. Rudenberg, *Rev. Mod. Phys.* **35**, 457 (1963).
- ³³M. W. Schmidt, K. K. Baldrige, J. A. Boatz, J. H. Jensen, S. Koseki, N. Matsunaga, M. S. Gordon, K. A. Nguyen, S. Su, T. L. Windus *et al.*, *J. Comput. Chem.* **14**, 1347 (1993).
- ³⁴F. A. Cotton and G. Wilkinson, *Advanced Inorganic Chemistry* (Wiley, New York, 1980).
- ³⁵J. H. Jensen and M. S. Gordon, *J. Phys. Chem.* **99**, 8091 (1995).
- ³⁶G. Burns, *Solid State Physics* (Academic Press, New York, 1985).
- ³⁷D. L. Mills, *Nonlinear Optics Basic Concepts* (Springer, New York, 1998).
- ³⁸G. van Rossum, *Python* (<http://www.python.org/>).
- ³⁹A. P. Mirgorodsky, T. Merle-Méjean, P. Thomas, J. C. Champarnaud-Mesjard, and B. Frit, *J. Phys. Chem. Solids* **63**, 545 (2002).
- ⁴⁰J. C. Champarnaud-Mesjard, P. Thomas, M. Colas-Dutreilh, and A. Oufkir, *Z. Kristallogr.* **216**, 185 (2001).
- ⁴¹M. Dutreilh, P. Thomas, J. C. Champarnaud-Mesjard, and B. Frit, *Solid State Sci.* **3**, 423 (2001).
- ⁴²B. Frit, D. Mercurio, P. Thomas, and J. C. Champarnaud-Mesjard, *Z. Kristallogr.* **214**, 439 (1999).
- ⁴³S. Blanchandin, J. C. Champarnaud-Mesjard, P. Thomas, and B. Frit, *J. Alloys Compd.* **306**, 175 (2000).
- ⁴⁴H. Sekino and J. Bartlett, *J. Chem. Phys.* **85**, 976 (1986).
- ⁴⁵S. J. A. van Gisbergen, J. G. Snijders, and E. J. Baerends, *Phys. Rev. Lett.* **78**, 3097 (1997).
- ⁴⁶T. Clark, J. Chandrasekhar, G. W. Spitznagel, and P. von R. Schleyer, *J. Comput. Chem.* **4**, 294 (1983).
- ⁴⁷S. Huzinaga, J. Andzelm, M. Klobulowski, E. Radzio-Andzelm, Y. Sakai, and H. Tatewaki, *Gaussian Basis Sets for Molecular Calculations* (Elsevier, New York, 1987).
- ⁴⁸S. Portmann and H. P. Lüthi, *Chimia* **54**, 766 (2000).